



Davey-Stewartson system and investigation of the impacts of the nonlinearity

Handenur Esen¹ · Ismail Onder¹ · Aydin Secer² · Muslum Ozisik¹ · Mustafa Bayram²

Received: 9 August 2023 / Accepted: 3 November 2023 / Published online: 27 December 2023
© The Author(s), under exclusive licence to Springer Science+Business Media, LLC, part of Springer Nature 2023

Abstract

This study examines for the first time the adapted parabolic law nonlinearity form of (2+1)-dimensional Davey-Stewartson system, an important equation modeling the surface water wave packets with finite depth. For the first time, we will investigate the parabolic law nonlinearity form. Not only is this a significant aspect, but we will also explore it with various parameter values to see its impact on soliton dynamics. In order to transform the nonlinear partial differential equation into a form for which the analytical method can be applied, the ordinary differential equation structure obtained by first applying wave transformation. In the following stage, we implement the new Kudryashov method and sinh-Gordon equation expansion techniques to retrieve bright, dark, singular, and different types of kink solitons. The effect of parabolic law nonlinearity parameters on the obtained soliton types has also been examined. We illustrate the 3D and 2D graphs of some of the obtained solutions to gain a physical perspective. The study will contribute to the literature in terms of the form of the examined problem, its content and results, and the effectiveness of the applied methods.

Keywords DSII equation · Surface tension · Soliton solution · The new Kudryashov method · sinh-Gordon equation expansion method

✉ Mustafa Bayram
mustafabayram@biruni.edu.tr

Handenur Esen
handenur@yildiz.edu.tr

Ismail Onder
ionder@yildiz.edu.tr

Aydin Secer
asecer@biruni.edu.tr

Muslum Ozisik
ozisik@yildiz.edu.tr

¹ Department of Mathematical Engineering, Yildiz Technical University, Istanbul, Turkey

² Department of Computer Engineering, Biruni University, Istanbul, Turkey

1 Introduction

Nonlinear partial differential equations (NLPDEs) are operated in order to model problems in various scientific and engineering areas. In addition to modeling NLPDEs, producing their analytical solutions is an area of great interest for researchers. Therefore, many techniques have been used in the literature to find the analytical solutions of NLPDEs like the F-expansion scheme (Ebaid and Aly 2012; Zhao 2013; Yıldırım 2021), Hirota bilinear approach (Hereman and Zhuang 1994; Satsuma 2003; Guo et al. 2020), the unified Riccati equation expansion method (Ozisk 2022; Cakicioglu et al. 2023; Ozisik et al. 2023; Esen et al. 2022), the generalized projective Riccati equations technique (Shahoot et al. 2018; Akram et al. 2021; Ozdemir 2022), enhanced Kudryashov method (Akbulut et al. 2022; Arnous et al. 2022; Arnous 2021; Arnous et al. 2022), generalized Kudryashov method (Arnous and Mirzazadeh 2016), the enhanced modified extended tanh expansion scheme (Onder et al. 2022; Ozisik et al. 2023), $\left(\frac{G'}{G^2}\right)$ -expansion method (Arshed and Raza 2020), $\exp(-\phi(\xi))$ -expansion method (Raza et al. 2023; Javid and Raza 2019; Raza et al. 2019), extended trial equation method (Raza and Javid 2019), trial equation method (Arnous et al. 2016).

Nonlinear evolution equations (NLEEs) model some of the nonlinear dynamical systems in the field of applied sciences such as optics (Mirzazadeh et al. 2015; Arnous and Moraru 2022; Arnous 2022), plasma (Debnath 1994; Whitham 2011). From these systems, the nonlinear Schrödinger equation (NLSE) is the most basic example of nonlinear integrable systems. NLSEs have been utilized to explain the ultrashort pulse propagation in the optical fiber and the slow evolution of a nonlinear weak wave packet in deep water (Peregrine 1983). Davey-Stewartson system (DSS) that was derived by Davey (1974) is an extension of the NLSE. The following $(2 + 1)$ -dimensional DSS is studied by many researchers for the surface water wave packets with finite depth (Davey 1974; Zedan and Monaquel 2010):

$$\begin{cases} i\phi_t + \frac{1}{2}\mu^2(\phi_{xx} + \mu^2\phi_{yy}) + \gamma|\phi|^2\phi - \psi_x\phi = 0, \\ \psi_{xx} - \mu^2\psi_{yy} - 2\gamma(|\phi|^2)_x = 0, \end{cases} \quad (1)$$

in which $\phi(x, y, t)$ denotes the amplitude of the wave packet of the surface, $\psi(x, y, t)$ is the velocity potential of the mean flow interacting with the surface wave; moreover, x, y represent the coordinates of the scaled spatial and t defines the coordinate of the scaled temporal. μ represents the surface tension, so $\mu = 1$ gives the DSI equation and $\mu = i$ gives the DSII equation (Sun et al. 2018). Furthermore, focusing or defocusing cases are described with $\gamma = \pm 1$. A general multiple-soliton solution form and the analytical traveling wave solutions for the DSS have been acquired via the simplest equation approach; besides, conservation law and the dispersion study have been analyzed in Selima et al. (2016). In Sun et al. (2018), through the Kadomtsev-Petviashvili hierarchy reduction, Sun et al. have produced the semi-rational solutions for eq. (1). Jafari et al. have obtained some novel analytical solutions including trigonometric and exponential functions for eq. (1) with the help of the first integral scheme in Jafari et al. (2012). Periodic and solitary wave solutions for the DSS have been derived through the sine-cosine approach in Zedan and Monaquel (2010). Gaballah et al. have produced the novel Jacobi elliptic wave function solutions of DSS utilizing the modified Jacobi elliptic function approach in Gaballah et al. (2022). Li et al. have acquired the lie symmetry algebra and some analytical solutions with the generalized

sub-equation expansion approach for a generalized DSS in Li et al. (2008). Dark, singular, bright, periodic, and rational solitary wave solutions of the generalized DSS have been acquired through the first integral scheme, $\exp(-\Phi(\xi))$ -expansion approach and first integral technique in Arshed et al. (2021). Moreover, the asymptotic attributes for the acquired family of the higher-order lump solutions of the DSII equation have been presented in Guo et al. (2022). Tang et al. introduced the resonant DSS in 2009 and its analytical solutions that define propagation, doubly periodic wave patterns have been produced with the multi-linear variable separation technique in Tang et al. (2009). Besides, for the $(2 + 1)$ -dimensional resonant DSS, it has been shown that the system is integrable by applying the Painleve test in Liang and Tang (2009). In order to derive bright, dark, and mixed dark-bright soliton solutions for the $(2 + 1)$ -dimensional resonant DSS, the sine-Gordon expansion technique has been utilized in Ismael et al. (2023). The new optical soliton solutions for the conformable coupled resonant DSS have been examined in Alabedalhadi et al. (2022) through the ansatz approach. Ismael et al. have produced dark, singular, bright, and singular solutions of the $(2 + 1)$ -dimensional resonant DSS with M-derivative in Ismael et al. (2021).

The new modified sine-Gordon technique has been used to get soliton solutions of variable-coefficient DSS in El-Shiekh and Gaballah (2020a). New Jacobi, periodic, and hyperbolic wave solutions have been retrieved for DSS with complex variable coefficients in El-Shiekh and Gaballah (2020b) via the direct similarity reduction technique.

The DSS was introduced as an extension of the NLSE. Although $(2 + 1)$ -dimensional DSS, generalized DSS, and resonant DSS have been studied before the parabolic law nonlinearity form has been adapted for the first time in this study. The $(2 + 1)$ -dimensional DSS (Ebadi et al. 2011) with the parabolic law nonlinearity is reads:

$$\begin{cases} i\phi_t + a(\phi_{xx} + \phi_{yy}) + b(c_1|\phi|^2 + c_2|\phi|^4)\phi - \alpha\phi\psi = 0, \\ \psi_{xx} + \psi_{yy} + \beta(d_1|\phi|^2 + d_2|\phi|^4)_{xx} = 0. \end{cases} \quad (2)$$

The $(2 + 1)$ -dimensional DSS is one of the complex member of NLPDEs that arises in the study of several physical phenomena including nonlinear optics, plasma physics, and fluid dynamics. The motivation for examining this model is that the presented system can allow estimable mathematical and physical insights into the behavior of solitons, waves, and other nonlinear structures. As is known, especially when it comes to events related to nonlinear optics and the models designed for them, one of the areas of focus is the controllability and management of soliton transmission. At the forefront of the factors affecting soliton transmission is nonlinearity, and in the last 20 years, various forms of nonlinearity, with the general heading of self-phase modulation, have found their place in the literature. Examples such as the parabolic law, power law, dual power law, polynomial law, cubic-quintic-septic law, anti-cubic law, triple power law, cubic-quintic-septic-ionic law, Kudryashov's law of refractive index, generalized anti-cubic law, and log law have been the subject of examination for many models in the literature. The primary focus is on controlling the form and amplitude of the soliton. In this context, the DSS model under investigation is also a widely studied area in the literature and has been the subject of many studies. Investigating the solutions and dynamics of the DSS with parabolic law may produce advancements in studying optical solitons and controlling wave patterns. Therefore, research in this area can have implications for solving real-world problems. The presented

model comprises physics, mathematics, and engineering concepts. Hence, another motivating point is that this study is interdisciplinary and creates connections between different branches of science. We emphasize that there is no study on eq. (2) in the literature; therefore, we aim to implement the new Kudryashov method (nKM) and sinh-Gordon equation expansion method (ShGEEM) to the $(2 + 1)$ -dimensional DSS with parabolic law to obtain the analytical solutions.

There are various analytical methods in order to acquire the analytical solutions of NLPDEs in the literature. We can classify these approaches in many different ways like allowing effective results, and ease of implementation, including different kinds of soliton solutions, not requiring too much mathematical processing. In fact, each method has its own advantages and disadvantages. Thus, the selection of the correct and appropriate method for the problem under consideration depends on the specific requirements and choice of the researcher for their analysis. However, in this article, the reasons for choosing the nKM for the presented model are its widespread use and ease of implementation. Moreover, ShGEEM retrieves more comprehensive and different types of solution functions and soliton types.

The remainder of this manuscript is organized as follows: In Sect. 2, utilizing the wave transformation we present the mathematical analysis for Eq. (2). The nKM and its implementation to Eq. (2) is offered in Sect. 3. We give the definition and application of ShGEEM in section 4. In Sect. 5, we achieve the stability analysis. The graphical illustrations and interpretations are represented in Sect. 6. Finally, we give the Conclusion in Sect. 7.

2 Mathematical analysis of the adapted system given in Eq. (2)

In this section, in order to produce the ordinary differential equation (ODE), we implement the following wave transformation:

$$\begin{aligned} \phi(x, y, t) &= U(\eta)e^{i\theta(x,y,t)}, \quad \psi(x, y, t) = V(\eta), \\ \theta(x, y, t) &= -\kappa_1 x - \kappa_2 y + \omega t + \Omega, \quad \eta = p_1 x + p_2 y - vt, \end{aligned} \quad (3)$$

in which $U(\eta)$ and $V(\eta)$ denote the scalar soliton profile for the complex ϕ and scalar ψ functions, respectively. $\theta(x, y, t)$ represents the phase component and p_1, p_2 are associated with the inverse widths of the soliton while v describes the velocity. κ_1 and κ_2 are the frequency of the soliton in the direction of x and y , respectively. While ω represents the wave number, Ω denotes the phase constant.

When we apply the wave transformation in eq. (3) to the first equation of Eq. (2), the following ODE is acquired:

$$a(p_1^2 + p_2^2)U'' - (a(\kappa_1^2 + \kappa_2^2) + \omega)U - \alpha UV + bc_1 U^3 + bc_2 U^5 = 0, \quad (4)$$

which comes from the real part while the imaginary part serves the condition as follows:

$$v = -2a(\kappa_1 p_1 + \kappa_2 p_2). \tag{5}$$

When we use the wave transformation in Eq. (3) for the second equation of Eq. (2), we get the following relation:

$$V(\eta) = -\frac{\beta p_1^2 U(\eta)^2 (d_2 U(\eta)^2 + d_1)}{p_1^2 + p_2^2}. \tag{6}$$

Substituting Eq. (6) into Eq. (4), we derive the following ODE:

$$a(p_1^2 + p_2^2)U'' - (a(\kappa_1^2 + \kappa_2^2) + \omega)U + \left(bc_1 + \frac{\alpha\beta p_1^2 d_1}{p_1^2 + p_2^2} \right)U^3 + \left(bc_2 + \frac{\alpha\beta p_1^2 d_2}{p_1^2 + p_2^2} \right)U^5 = 0. \tag{7}$$

When applying the homogeneous balance rule between the highest order terms U'' and U^5 , we get $m + 2 = 5m$, that is $m = \frac{1}{2}$. Since the m is the balance number and it is considered as positive integer, we need to define the following simple transformation:

$$U = \sqrt{P}, \tag{8}$$

where $P = P(\eta)$ is a new function. When we substitute Eqs. (8) into (7), we have the following equation:

$$a(p_1^2 + p_2^2)^2 (P')^2 - 2a(p_1^2 + p_2^2)^2 PP'' + 4(p_1^2 + p_2^2) [(\kappa_1^2 + \kappa_2^2)a + \omega] P^2 + [4(-\alpha\beta d_1 - bc_1)p_1^2 - 4p_2^2 bc_1] P^3 + [4(-\alpha\beta d_2 - bc_2)p_1^2 - 4p_2^2 bc_2] P^4 = 0. \tag{9}$$

Finally, balancing the terms PP'' and P^4 , the balancing constant is found as $m = 1$.

3 Explanation and implementation of nKM

In this section, the presentation and application of the nKM method (Kudryashov 2020; Ozisik et al. 2022; Albayrak 2023), which is the first of the methods to be used in the article, are provided. One of the reasons for choosing the nKM method is that it is a contemporary method, easily applicable, secure, and has the capability to produce bright, dark, and singular soliton solutions, which are among the fundamental soliton types. The nKM method, like many methods commonly used in the literature, is based on an auxiliary differential equation, and many methods that use the same auxiliary equation have been used

in the literature in recent years. Moreover, many of these methods contain a large number of solution functions. At this point, one of the advantages of the nKM method is that it does not contain repeating soliton solutions. Additionally, the ability of the nKM to be applied to a wide range of NLPDE equations constitutes another advantageous point. These fundamental features have been the main factors in selecting the nKM method. The nKM (Kudryashov 2020; Ozisik et al. 2022; Albayrak 2023) offers that the solution of eq. (2) in the following structure:

$$P(\eta) = \sum_{s=0}^m \Lambda_s \vartheta^s(\eta), \tag{10}$$

in which Λ_s are real constants to be determined, provided that $\Lambda_m \neq 0$. m denotes the balancing constant found as $m = 1$ in eq. (2). Therefore, eq. (10) becomes,

$$P(\eta) = \Lambda_0 + \Lambda_1 \vartheta(\eta), \tag{11}$$

where $\vartheta(\eta)$ is the solution of the following formula:

$$\vartheta'^2(\eta) = \delta^2 \vartheta^2(\eta) [1 - \lambda \vartheta^2(\eta)], \tag{12}$$

in which δ and λ are real values. Additionally, the solution of eq. (12) is given as follows (Kudryashov 2020; Ozisik et al. 2022):

$$\vartheta(\eta) = \frac{4\tau}{4\tau^2 e^{\delta\eta} + \lambda e^{-\delta\eta}}, \tag{13}$$

in which τ is a nonzero constant. Equation (13) gives the bright soliton when $\lambda = 4\tau^2$ and the singular soliton for $\lambda = -4\tau^2$.

When substituting Eqs. (11) with (12) into Eq. (9), collecting all $\vartheta^s(\eta)$ coefficients and equating them to zero, we reach the following algebraic system:

$$\begin{aligned} \vartheta^0(\eta) &: ((-Mp_1^2 - p_2^2 bc_2)\Lambda_0^2 + (-Np_1^2 - p_2^2 bc_1)\Lambda_0 + S(aR + \omega))\Lambda_0^2 = 0, \\ \vartheta^1(\eta) &: (8(Mp_1^2 + p_2^2 bc_2)\sigma_0^2 + 6(Np_1^2 + p_2^2 bc_1)\sigma_0 + (a\delta^2 S - 4aR - 4\omega)S)\Lambda_1\Lambda_0 = 0, \\ \vartheta^2(\eta) &: (24(Mp_1^2 + p_2^2 bc_2)\Lambda_0^2 + 12(Np_1^2 + p_2^2 bc_1)\Lambda_0 + (a\delta^2 S - 4aR - 4\omega)S)\Lambda_1^2 = 0, \\ \vartheta^3(\eta) &: ((-4(Mp_1^2 + p_2^2 bc_2)\Lambda_0 - Np_1^2 - p_2^2 bc_1)\Lambda_1^2 + a\delta^2 \lambda S^2 \Lambda_0)\Lambda_1 = 0, \\ \vartheta^4(\eta) &: (-4(Mp_1^2 + p_2^2 bc_2)\Lambda_1^2 + 3a\delta^2 \lambda S^2)\Lambda_1^2 = 0, \end{aligned} \tag{14}$$

where $M = (\alpha\beta d_2 + bc_2)$, $N = (\alpha\beta d_1 + bc_1)$, $S = (p_1^2 + p_2^2)$ and $R = (\kappa_1^2 + \kappa_2^2)$. The solution sets of eq. (14) are derived as follows: **Set 1:**

$$p_1 = \sqrt{\frac{-bc_1}{N}} p_2, \quad \Lambda_0 = 0, \quad \Lambda_1 = \sqrt{\frac{-3\lambda d_1(aR+\omega)}{bK}}, \quad \delta = 2\sqrt{\frac{(aR+\omega)N}{\alpha\alpha\beta d_1 p_2^2}}, \tag{15}$$

Set 2:

$$\omega = \frac{-3aR\lambda d_1 - bK\Lambda_1^2}{3d_1\lambda}, \quad \Lambda_1 = \Lambda_1, \quad p_1 = \frac{2b\Lambda_1\sqrt{3\alpha\alpha\beta\lambda c_1 K}}{3\alpha\alpha\beta\lambda\delta d_1}, \quad p_2 = \frac{2\Lambda_1\sqrt{-3\alpha\alpha\beta\lambda bKN}}{3\alpha\alpha\beta\lambda\delta d_1}, \tag{16}$$

$$\kappa_1 = \kappa_1, \quad \kappa_2 = \kappa_2, \quad \Lambda_0 = 0,$$

Set 3:

$$\lambda = -\frac{4b\Lambda_1^2 KN}{3\alpha\alpha\beta p_2^2 d_1^2 \delta^2}, \quad \omega = -\frac{a[\beta d_1(-p_2^2\delta^2+4R)\alpha+4bc_1R]}{4N}, \quad p_1 = \sqrt{\frac{-bc_1}{N}} p_2, \tag{17}$$

$$p_2 = p_2, \quad \Lambda_0 = 0, \quad \Lambda_1 = \Lambda_1$$

Set 4:

$$\lambda = \frac{4c_1\Lambda_1^2 b^2 K}{3\alpha\alpha\beta d_1^2 \delta^2 p_1^2}, \quad \omega = -\frac{a[4bc_1 R+\alpha\beta d_1 \delta^2 p_1^2]}{4bc_1}, \quad \delta = \delta, \quad p_2 = \sqrt{-\frac{N}{bc_1}} p_1, \quad \Lambda_0 = 0, \quad \Lambda_1 = \Lambda_1. \tag{18}$$

where $K = (c_1 d_2 - c_2 d_1)$. After we substitute the sets in Eqs. (15)–(18) into Eq. (11) with Eq. (13) and utilize Eqs. (3), (8), we acquire the following analytical solutions for Eq. (2):

$$\phi_{1,1}(x, y, t) = \left(\frac{4\sqrt{\frac{-3\lambda d_1(aR+\omega)}{bK}} \tau}{4\tau^2 e^{\delta\eta} + \lambda e^{-\delta\eta}} \right)^{\frac{1}{2}} \times e^{i(\omega t - x\kappa_1 - y\kappa_2 + \Omega)}, \tag{19}$$

$$\psi_{1,1}(x, y, t) = -\frac{4\beta\tau p_1^2}{S} \left(\frac{\sqrt{\frac{-3\lambda d_1(aR+\omega)}{bK}}}{4\tau^2 e^{\delta\eta} + \lambda e^{-\delta\eta}} \right) \left(d_1 + d_2 \left(\frac{4\sqrt{\frac{-3\lambda d_1(aR+\omega)}{bK}} \tau}{4\tau^2 e^{\delta\eta} + \lambda e^{-\delta\eta}} \right) \right), \tag{20}$$

where p_1, δ are given in eq. (15).

$$\phi_{1,2}(x, y, t) = \sqrt{\frac{4\Lambda_1 \tau}{4\tau^2 e^{\delta\eta} + \lambda e^{-\delta\eta}}} \times e^{i\left(\frac{-3aR\lambda d_1 - bK\Lambda_1^2}{3d_1\lambda} t - x\kappa_1 - y\kappa_2 + \Omega\right)}, \tag{21}$$

$$\psi_{1,2}(x, y, t) = -\frac{\beta p_1^2}{S} \left(\frac{4\Lambda_1 \tau}{4\tau^2 e^{\delta\eta} + \lambda e^{-\delta\eta}} \right) \left(d_1 + d_2 \left(\frac{4\Lambda_1 \tau}{4\tau^2 e^{\delta\eta} + \lambda e^{-\delta\eta}} \right) \right), \tag{22}$$

where p_1, p_2 are described in Eq. (16).

$$\phi_{1,3}(x, y, t) = \left(\frac{4\Lambda_1 \tau}{4\tau^2 e^{\delta\eta} - \frac{4b\Lambda_1^2 KN}{3\alpha\alpha\beta p_2^2 d_1^2 \delta^2} e^{-\delta\eta}} \right)^{\frac{1}{2}} \times e^{i\left(-\frac{a[\beta d_1(-p_2^2\delta^2+4R)\alpha+bc_1R]}{4N} t - x\kappa_1 - y\kappa_2 + \Omega\right)}, \tag{23}$$

$$\psi_{1,3}(x, y, t) = -\frac{\beta p_1^2}{S} \left(\frac{4\Lambda_1 \tau}{4\tau^2 e^{\delta\eta} - \frac{4b\Lambda_1^2 KN}{3\alpha\alpha\beta p_2^2 d_1^2 \delta^2} e^{-\delta\eta}} \right) \left(d_1 + d_2 \left(\frac{4\Lambda_1 \tau}{4\tau^2 e^{\delta\eta} - \frac{4b\Lambda_1^2 KN}{3\alpha\alpha\beta p_2^2 d_1^2 \delta^2} e^{-\delta\eta}} \right) \right), \tag{24}$$

where p_1 is given in Eq. (17).

$$\phi_{1,4}(x, y, t) = \left(\frac{4\Lambda_1 \tau}{4\tau^2 e^{\delta\eta} + \frac{4c_1 \Lambda_1^2 b^2 K}{3\alpha\alpha\beta d_1^2 \delta^2 p_1^2} e^{-\delta\eta}} \right)^{\frac{1}{2}} \times e^{i \left(-\frac{a[4bc_1 R + \alpha\beta d_1 \delta^2 p_1^2]}{4bc_1} t - x\kappa_1 - y\kappa_2 + \Omega \right)}, \tag{25}$$

$$\psi_{1,4}(x, y, t) = -\frac{\beta p_1^2}{S} \left(\frac{4\Lambda_1 \tau}{4\tau^2 e^{\delta\eta} + \frac{4c_1 \Lambda_1^2 b^2 K}{3\alpha\alpha\beta d_1^2 \delta^2 p_1^2} e^{-\delta\eta}} \right) \left(d_1 + d_2 \left(\frac{4\Lambda_1 \tau}{4\tau^2 e^{\delta\eta} + \frac{4c_1 \Lambda_1^2 b^2 K}{3\alpha\alpha\beta d_1^2 \delta^2 p_1^2} e^{-\delta\eta}} \right) \right), \tag{26}$$

where p_2 is represented in Eq. (18). In Eqs. (19)–(26), $v = -2a(\kappa_1 p_1 + \kappa_2 p_2)$, $\eta = p_1 x + p_2 y - vt$ which are given in Eqs. (5) and (3), respectively.

4 Description and enforcement of ShGEEM

In this section, efforts are being made to introduce and implement the ShGEEM, which is chosen as the second method (Yan 2003a, b; Mathanaranjan et al. 2022; Seadawy et al. 2018; Kumar et al. 2018; Foroutan et al. 2018; Kumar et al. 2018, 2019). In addition to being an effective method, the SHGEEM also has the capability to be applied to many problems. The ease of application and reliability of the method are among its other advantages. We take into account the following solution form in order to apply the proposed scheme:

$$P(\Theta) = \sigma_0 + \sum_{s=1}^m \cosh^{s-1}(\Theta) [\sigma_s \cosh(\Theta) + \Upsilon_s \sinh(\Theta)], \tag{27}$$

where σ_s and Υ_s are real values. Moreover, $\Theta = \Theta(\eta)$ satisfies the following equation:

$$\frac{d\Theta}{d\eta} = \sqrt{\sinh^2(\Theta) + C}, \tag{28}$$

where C represents the integration constant. Considering the $C = 0$, eq. (28) gives the following solutions:

$$\sinh(\Theta) = \operatorname{csch}(\eta), \quad \cosh(\Theta) = \operatorname{coth}(\eta), \tag{29}$$

$$\sinh(\Theta) = \operatorname{isech}(\eta), \quad \cosh(\Theta) = \operatorname{tanh}(\eta). \tag{30}$$

Since we determined the balancing constant as $m = 1$ in eq. (2), therefore, eq. (27) converts into:

$$P(\Theta) = \sigma_0 + \sigma_1 \cosh(\Theta) + \Upsilon_1 \sinh(\Theta). \tag{31}$$

After substituting Eqs. (31) and (28) into Eq. (9), we produce a polynomial. If the coefficients of $\cosh^i(\Theta)\sinh^j(\Theta)$, $i = 0, \dots, 4$, $j = 0, 1$ are equated to zero, the following algebraic system is derived:

$$\begin{aligned}
 & \cosh^0(\Theta)\sinh^0(\Theta): \left[(-24M\sigma_0^2 - 12N\sigma_0 + 4ap_2^2 + 4aR + 4\omega)p_1^2 + 2ap_1^4 \right. \\
 & + 2p_2^2(-12\sigma_0^2bc_2 - 6\sigma_0bc_1 + ap_2^2 + 2aR + 2\omega) \left. \right] Y_1^2 + 4(Mp_1^2 + p_2^2bc_2) Y_1^4 \\
 & - p_2^2(ap_2^2\sigma_1^2 + 4\sigma_0^2(-\sigma_0^2bc_2 - \sigma_0bc_1 + aR + \omega)) - ap_1^4\sigma_1^2 \\
 & + [-2ap_2^2\sigma_1^2 - 4(-M\sigma_0^2 - N\sigma_0 + aR + \omega)\sigma_0^2] p_1^2 = 0, \\
 \\
 & \cosh^0(\Theta)\sinh^1(\Theta): \\
 & \left. \left(\begin{aligned} & 2 \left[(4M\sigma_0 + N)p_1^2 + 4p_2^2 \left(\sigma_0c_2 + \frac{c_1}{4} \right) b \right] Y_1^2 \right. \\ & + \left[(-8M\sigma_0^2 - 6N\sigma_0 + 2ap_2^2 + 4(aR + \omega)) p_1^2 \right. \\ & \left. \left. + ap_1^4 + (-8\sigma_0^2bc_2 - 6\sigma_0bc_1 + ap_2^2 + 4(aR + \omega)) p_2^2 \right] \sigma_0 \right) \right\} Y_1 = 0, \\
 \\
 & \cosh^1(\Theta)\sinh^0(\Theta): \\
 & \left. \left(\begin{aligned} & 3 \left((4M\sigma_0 + N)p_1^2 + 4p_2^2 \left(\sigma_0c_2 + \frac{c_1}{4} \right) b \right) Y_1^2 \right. \\ & + \left[(-4M\sigma_0^2 - 3N\sigma_0 + 2ap_2^2 + 2aR + 2\omega) p_1^2 + ap_1^4 \right. \\ & \left. \left. + p_2^2 \left(-4\sigma_0^2bc_2 - 3\sigma_0bc_1 + ap_2^2 + 2aR + 2\omega \right) \right] \sigma_0 \right) \right\} \sigma_1 = 0, \\
 \\
 & \cosh^1(\Theta)\sinh^1(\Theta): \\
 & \left. \left(\begin{aligned} & 4(Mp_1^2 + p_2^2bc_2) Y_1^2 + [-12M\sigma_0^2 - 6N\sigma_0 + 2ap_2^2 + 2aR + 2\omega] p_1^2 \right) \sigma_1 Y_1 = 0, \\ & + ap_1^4 + [-12\sigma_0^2bc_2 - 6\sigma_0bc_1 + ap_2^2 + 2aR + 2\omega] p_2^2 \right) \\
 \\
 & \cosh^2(\Theta)\sinh^0(\Theta): -8 \left((\alpha\beta d_2 + c_2b) p_1^2 + p_2^2bc_2 \right) Y_1^4 \\
 & - 2 \left(\begin{aligned} & (-12M\sigma_0^2 - 6N\sigma_0 + 2ap_2^2 + 2aR + 2\omega) p_1^2 \\ & + ap_1^4 + p_2^2(-12\sigma_0^2bc_2 - 6\sigma_0bc_1 + ap_2^2 + 2aR + 2\omega) \end{aligned} \right) \sigma_1^2 \\
 & + \left(\begin{aligned} & (-24M\sigma_1^2 + 24M\sigma_0^2 + 12N\sigma_0 - 10ap_2^2 - 4aR - 4\omega) p_1^2 - 5ap_1^4 \\ & - p_2^2(24(c_2b\sigma_1^2 - \sigma_0^2bc_2) - 12\sigma_0bc_1 + 5ap_2^2 + 4aR + 4\omega) \end{aligned} \right) Y_1^2 = 0, \\
 \\
 & \cosh^2(\Theta)\sinh^1(\Theta): \\
 & \left. \left(\begin{aligned} & (4M\sigma_0 + N)p_1^2 + p_2^2(4\sigma_0c_2 + c_1)b \right) Y_1^2 + (3(4M\sigma_0 + N)\sigma_1^2 + 2ap_2^2\sigma_0) p_1^2 \right) \\ & + a\sigma_0p_1^4 + p_2^2(12(\sigma_0c_2 + \frac{c_1}{4})b\sigma_1^2 + ap_2^2\sigma_0) \left. \right\} Y_1 = 0, \\
 \\
 & \cosh^3(\Theta)\sinh^0(\Theta): \\
 & \left. \left(\begin{aligned} & 3 \left[(4M\sigma_0 + N)p_1^2 + 4p_2^2 \left(\sigma_0c_2 + \frac{c_1}{4} \right) b \right] Y_1^2 + (4M\sigma_0 + N)\sigma_1^2 + 2ap_2^2\sigma_0 \right) p_1^2 \right. \\ & \left. + p_2^2 \left((4\sigma_0c_2 + c_1)b\sigma_1^2 + ap_2^2\sigma_0 \right) + a\sigma_0p_1^4 \right) \right\} \sigma_1 = 0, \\
 \\
 & \cosh^3(\Theta)\sinh^1(\Theta): \\
 & \left((8Mp_1^2 + 8p_2^2bc_2) Y_1^2 + (8M\sigma_1^2 + 6ap_2^2) p_1^2 + (8c_2b\sigma_1^2 + 3ap_2^2) p_2^2 + 3ap_1^4 \right) \sigma_1 Y_1 = 0, \\
 \\
 & \cosh^4(\Theta)\sinh^0(\Theta): \\
 & 3(ap_1^4 + (8M\sigma_1^2 + 2ap_2^2) p_1^2 + 8p_2^2\sigma_1^2bc_2 + ap_2^4) Y_1^2 + 4(Mp_1^2 + p_2^2bc_2) Y_1^4 \\
 & + (3ap_1^4 + (4M\sigma_1^2 + 6ap_2^2) p_1^2 + p_2^2(4c_2b\sigma_1^2 + 3ap_2^2)) \sigma_1^2 = 0,
 \end{aligned}
 \tag{32}$$

where $M = (\alpha\beta d_2 + bc_2)$, $N = (\alpha\beta d_1 + bc_1)$, $S = (p_1^2 + p_2^2)$ and $R = (\kappa_1^2 + \kappa_2^2)$. Solving the system given in Eq. (32), the solution sets are retrieved as follows:

Family 1:

$$\begin{aligned}
 d_1 &= \frac{(2aS - bc_1\sigma_1)S}{\sigma_1\alpha\beta p_1^2}, \quad d_2 = -\frac{(4c_2b\sigma_1^2 + 3aS)S}{4\alpha\beta p_1^2\sigma_1^2}, \quad \omega = a(S - R), \\
 p_1 &= p_1, \quad p_2 = p_2, \quad \sigma_0 = \sigma_1, \quad \sigma_1 = \sigma_1, \quad Y_1 = 0.
 \end{aligned}
 \tag{33}$$

Family 2:

$$\omega = \frac{(-Y_1^2 bc_2 - 3aR)d_1 + bc_1 d_2 Y_1^2}{3d_1}, P_1 = \frac{2\sqrt{-3a\alpha\beta c_1 K} Y_1 b}{3a\alpha\beta d_1}, P_2 = \frac{2\sqrt{3a\alpha\beta bKN} Y_1}{3a\alpha\beta d_1}, \quad (34)$$

$$\kappa_1 = \kappa_1, \kappa_2 = \kappa_2, \sigma_0 = 0, \sigma_1 = 0, Y_1 = Y_1.$$

Family 3:

$$c_1 = \frac{-2\alpha\beta d_1 p_1^2 \sigma_1 + ap_1^4 + 2p_1^2 ap_2^2 + ap_2^4}{2\sigma_1 bS}, c_2 = \frac{-16p_1^2 \sigma_1^2 \alpha\beta d_2 - 3ap_1^4 - 6p_1^2 ap_2^2 - 3ap_2^4}{16b\sigma_1^2 S}, \omega = \frac{a(p_1^2 + p_2^2 - 4\kappa_1^2 - 4\kappa_2^2)}{4}, \quad (35)$$

$$\sigma_0 = \sigma_1, \sigma_1 = \sigma_1, Y_1 = \sigma_1,$$

where $K = (c_1 d_2 - c_2 d_1)$. If Eqs. (33), (34), (35) are substituted into Eq. (31) by considering Eqs. (3), (8), (29), (30) the following solutions are acquired:

-With the set in Eq. (33):

$$\phi_{2,1}(x, y, t) = \sqrt{-\sigma_1(\coth(\eta) - 1)} e^{i((S-R)at - \kappa_1 x - \kappa_2 y + \Omega)}, \quad (36)$$

$$\psi_{2,1}(x, y, t) = \frac{(4bc_2\sigma_1^2 \coth(\eta) + 3a \coth(\eta)S - 4c_2 b\sigma_1^2 + 5ap_1^2 + 5ap_2^2 - 4bc_1\sigma_1)(\coth(\eta) - 1)}{4\alpha}, \quad (37)$$

$$\phi_{2,2}(x, y, t) = \sqrt{\sigma_1(\tanh(\eta) + 1)} e^{i((S-R)at - \kappa_1 x - \kappa_2 y + \Omega)}, \quad (38)$$

$$\psi_{2,2}(x, y, t) = \frac{(4bc_2\sigma_1^2 \tanh(\eta) + 3aS \tanh(\eta) + 4c_2 b\sigma_1^2 - 5aS + 4bc_1\sigma_1)(\tanh(\eta) + 1)}{4\alpha}. \quad (39)$$

-With the set in Eq. (34):

$$\phi_{2,3}(x, y, t) = \sqrt{\frac{Y_1}{\sinh(\eta)}} \times e^{i\left(\frac{(-(bc_2 Y_1^2 + 3aR) - 3(\kappa_1 x + \kappa_2 y - \Omega))d_1 + bc_1 d_2 Y_1^2}{3d_1}\right)}, \quad (40)$$

$$\psi_{2,3}(x, y, t) = \frac{(d_1 \sinh(\eta) + d_2 Y_1)c_1 Y_1 b}{\sinh(\eta)^2 \alpha d_1}, \quad (41)$$

$$\phi_{2,4}(x, y, t) = \sqrt{\frac{Y_1 i}{\cosh(\eta)}} \times e^{i\left(\frac{(-(bc_2 Y_1^2 + 3aR) - 3(\kappa_1 x + \kappa_2 y - \Omega))d_1 + bc_1 d_2 Y_1^2}{3d_1}\right)}, \quad (42)$$

$$\psi_{2,4}(x, y, t) = \frac{i(d_2 Y_1 + d_1 \cosh(\eta))c_1 Y_1 b}{\cosh(\eta)^2 \alpha d_1}. \quad (43)$$

-With the set in Eq. (35):

$$\phi_{2,5}(x, y, t) = \sqrt{\frac{\sigma_1(1 - \cosh(\eta) + \sinh(\eta))}{\sinh(\eta)}} \times e^{i\left(\frac{a(S-4R)t}{4} - \kappa_1 x - \kappa_2 y + \Omega\right)}, \quad (44)$$

$$\psi_{2,5}(x, y, t) = -\frac{p_1^2 \beta \sigma_1 ((2d_2 \sigma_1 + d_1) \cosh(\eta) - (2d_2 \sigma_1 + d_1) \sinh(\eta) + d_1)}{(\cosh(\eta) + 1)(p_1^2 + p_2^2)} \quad (45)$$

$$\phi_{2,6}(x, y, t) = \sqrt{\frac{\sigma_1(i + \sinh(\eta) + \cosh(\eta))}{\cosh(\eta)}} \times e^{i\left(\frac{a(S-4R)t}{4} - \kappa_1 x - \kappa_2 y + \Omega\right)}, \quad (46)$$

$$\psi_{2,6}(x, y, t) = -\frac{p_1^2 \beta \sigma_1 (-2d_2 \sigma_1 + d_1) \sinh(\eta) - (2d_2 \sigma_1 + d_1) \cosh(\eta) + id_1}{(-\sinh(\eta) + i)\delta}. \tag{47}$$

In Eqs.(36)–(47) $v = -2a(p_1 \kappa_1 + p_2 \kappa_2)$ and $\eta = -vt + p_1 x + p_2 y$.

It can be declared that all the acquired solutions satisfy the presented system. Although Eqs. (42),(43), (46) and (47) are solutions offered by the ShGEEM and given mathematically, they have not been evaluated in the article due to the definition given in Eq. (3).

5 Modulation instability

Substitute the followings into the Eq. (2);

$$\begin{aligned} \phi(x, y, t) &= (\Phi_0 + \epsilon \Phi_1(x, y, t)) e^{-i\Psi_0 t}, \\ \psi(x, y, t) &= \Psi_0 + \epsilon \Psi_1(x, y, t), \end{aligned} \tag{48}$$

where Φ_0 and Ψ_0 are normalized optical power. Then linearized equations in terms of $\Phi_1(x, y, t)$ and $\Psi_1(x, y, t)$ are obtained as follows;

$$\begin{aligned} \epsilon \left(a \left(\frac{\partial^2}{\partial x^2} \Phi_1 \right) + a \left(\frac{\partial^2}{\partial y^2} \Phi_1 \right) \right. \\ \left. + i \left(\frac{\partial}{\partial t} \Phi_1 \right) + ((5bc_2 \Phi_0^3 + 3bc_1 \Phi_0 + 1)\Phi_0 - \alpha \Psi_0)\Phi_1 - \alpha \Psi_1 \Phi_0 \right) = 0, \\ \epsilon \left(\frac{\partial^2}{\partial x^2} \Psi_1 + \frac{\partial^2}{\partial y^2} \Psi_1 + 2\beta d_1 \left(\frac{\partial^2}{\partial x^2} \Phi_1 \right) \Phi_0 + 4\beta d_2 \left(\frac{\partial^2}{\partial x^2} \Phi_1 \right) \Phi_0^3 \right) = 0. \end{aligned} \tag{49}$$

Substitute the followings into the linearized PDEs in Eq. (49):

$$\begin{aligned} \Phi_1(x, y, t) &= A_1 e^{i(\omega t - x\kappa_1 - y\kappa_2)} + A_2 e^{-i(\omega t - x\kappa_1 - y\kappa_2)}, \\ \Psi_1(x, y, t) &= B_1 e^{i(\omega t - x\kappa_1 - y\kappa_2)} + B_2 e^{-i(\omega t - x\kappa_1 - y\kappa_2)}, \end{aligned} \tag{50}$$

where ω , κ_1 and κ_2 are real values. Collecting the coefficients of $e^{i(\omega t - x\kappa_1 - y\kappa_2)}$ and $e^{-i(\omega t - x\kappa_1 - y\kappa_2)}$ and create a coefficient matrix as follows:

$$M = \begin{bmatrix} M_{11} & M_{12} \\ M_{21} & M_{22} \end{bmatrix}, \tag{51}$$

where

$$\begin{aligned} M_{11} &= 5bc_2 \Phi_0^4 \epsilon A_2 + 3bc_1 \Phi_0^2 \epsilon A_2 - a\epsilon A_2 \kappa_1^2 - a\epsilon A_2 \kappa_2^2 - \alpha \Psi_0 \epsilon A_2 - \alpha \epsilon B_2 \Phi_0 + \Phi_0 \epsilon A_2 + \epsilon A_2 \omega, \\ M_{12} &= 5A_1 \Phi_0^4 bc_2 \epsilon + 3A_1 \Phi_0^2 bc_1 \epsilon - A_1 a \epsilon \kappa_1^2 - A_1 a \epsilon \kappa_2^2 - A_1 \Psi_0 \alpha \epsilon - B_1 \Phi_0 \alpha \epsilon + A_1 \Phi_0 \epsilon - A_1 \epsilon \omega, \\ M_{21} &= -4\beta d_2 \epsilon A_2 \kappa_1^2 \Phi_0^3 - 2\beta d_1 \epsilon A_2 \kappa_1^2 \Phi_0 - \epsilon B_2 \kappa_1^2 - \epsilon B_2 \kappa_2^2, \\ M_{22} &= -4A_1 \Phi_0^3 \beta d_2 \epsilon \kappa_1^2 - 2A_1 \Phi_0 \beta d_1 \epsilon \kappa_1^2 - B_1 \epsilon \kappa_1^2 - B_1 \epsilon \kappa_2^2. \end{aligned} \tag{52}$$

Solve the ω in Eq. (51) in according to $\det(M) = 0$:

$$\omega = \frac{-(A_1B_2 - A_2B_1)(a\kappa_1^4 + \Omega_1\kappa_1^2 + \Omega_2\kappa_2^2)}{\Omega_3\kappa_1^2 + \kappa_2^2(A_1B_2 + A_2B_1)}, \tag{53}$$

where

$$\begin{aligned} \Omega_1 &= (-4\alpha\beta d_2 - 5bc_2)\Phi_0^4 + (-2\alpha\beta d_1 - 3bc_1)\Phi_0^2 - \Phi_0 + 2a\kappa_2^2 + \alpha\Psi_0, \\ \Omega_2 &= -5bc_2\Phi_0^4 - 3bc_1\Phi_0^2 + a\kappa_2^2 + \alpha\Psi_0 - \Phi_0, \\ \Omega_3 &= 8A_1A_2\Phi_0^3\beta d_2 + 4A_1A_2\Phi_0\beta d_1 + A_1B_2 + A_2B_1. \end{aligned} \tag{54}$$

Since Eq. (53) does not have a structure containing any complex form, it does not have an instability state. Therefore, modulation instability does not occur and the solutions of Eq. (2) are stable.

6 Results and discussion

In this section, we showcase our results through graphical illustrations and provide interpretations of the gathered insights. Figs. 1a and 1b illustrate the 3D portraits for $|\phi_{1,1}(x, 1, t)|$ and $\psi_{1,1}(x, 1, t)$ at $\tau = 2, c_1 = 2, d_1 = 1, c_2 = 0.3, d_2 = 1, a = 1, b = -0.4, \kappa_1 = 2, \kappa_2 = 1, \alpha = 1, \beta = 2, \omega = 1, \lambda = 16, p_2 = 2, \Omega = 1$. We plot the 2D graphs in Fig. 1c–f to investigate the effects of the parameters c_1, c_2, d_1 and d_2 to the behavior of the soliton. The 2D views of $|\phi_{1,1}(x, 1, 1)|$ (continuous lines) and $\psi_{1,1}(x, 1, 1)$ (dashed lines) at $\tau = 2, d_1 = 1, c_2 = 0.3, d_2 = 1, a = 1, b = -0.4, \kappa_1 = 2, \kappa_2 = 1, \alpha = 1, \beta = 2, \omega = 1, \lambda = 16, p_2 = 2, \Omega = 1$ for $c_1 = 0.5, 0.75, 1.5$ is depicted in Fig. 1c. We demonstrate the 2D plots of $|\phi_{1,1}(x, 1, 1)|$ (continuous lines) and $\psi_{1,1}(x, 1, 1)$ (dashed lines) at $\tau = 2, d_1 = 1, c_1 = 2, d_2 = 1, a = 1, b = -0.4, \kappa_1 = 2, \kappa_2 = 1, \alpha = 1, \beta = 2, \omega = 1, \lambda = 16, p_2 = 2, \Omega = 1$ for $c_2 = 0.25, 0.75, 1.5$ in Fig. 1d. The 2D views of $|\phi_{1,1}(x, 1, 1)|$ (continuous lines) and $\psi_{1,1}(x, 1, 1)$ (dashed lines) at $\tau = 2, c_1 = 2, c_2 = 0.3, d_2 = 1, a = 1, b = -0.4, \kappa_1 = 2, b = -0.4, \kappa_1 = 2, \kappa_2 = 1, \alpha = 1, \kappa_2 = 1, \alpha = 1, \beta = 2, \omega = 1, \lambda = 16, p_2 = 2, \Omega = 1$ for $d_1 = 1, 2, 3$ is plotted in Fig. 1e. We illustrate the 2D plots of $|\phi_{1,1}(x, 1, 1)|$ (continuous lines) and $\psi_{1,1}(x, 1, 1)$ (dashed lines) at $\tau = 2, d_1 = 1, c_1 = 2, c_2 = 0.3, a = 1, \beta = 2, \omega = 1, \lambda = 16, p_2 = 2, \Omega = 1$ for $d_2 = 0.25, 0.5, 1$ in Fig. 1f. We can observe that Fig. 1 represents the bright soliton for $|\phi_{1,1}(x, 1, t)|$ and the dark soliton for $\psi_{1,1}(x, 1, t)$. For increasing values of c_1 in Fig. 1c, we can see that both the soliton represented with $|\phi_{1,1}(x, 1, 1)|$ moves to the right and the amplitude of the soliton decreases. Depending on the increasing values of c_1 , the shape of the soliton turns into a more degenerate form, in a sense it gives a view whose apex approaches the horizontal axis. A similar view occurs for Fig. 1e but for decreasing values of d_1 . In Figs. 1d and f, the observation obtained with the previous examination is followed for increasing values of c_2 and decreasing values of d_2 without observing any horizontal movement of the soliton. However, the form of the soliton gives the view of more deformation in both graphs, that is, a view almost approaching the horizontal axis is formed. It is seen from Fig. 1c that the amplitude of the dark soliton decreases and moves to the right depending on the increasing values of c_1 for $\psi_{1,1}(x, 1, 1)$. A similar behavior occurs for decreasing values of d_1 in Fig. 1e. On the other hand, the amplitude of the soliton increases depending on the increase in c_2 without a horizontal position change in Fig. 1d. A similar view appears due to decreasing values of d_2 in Fig. 1f.

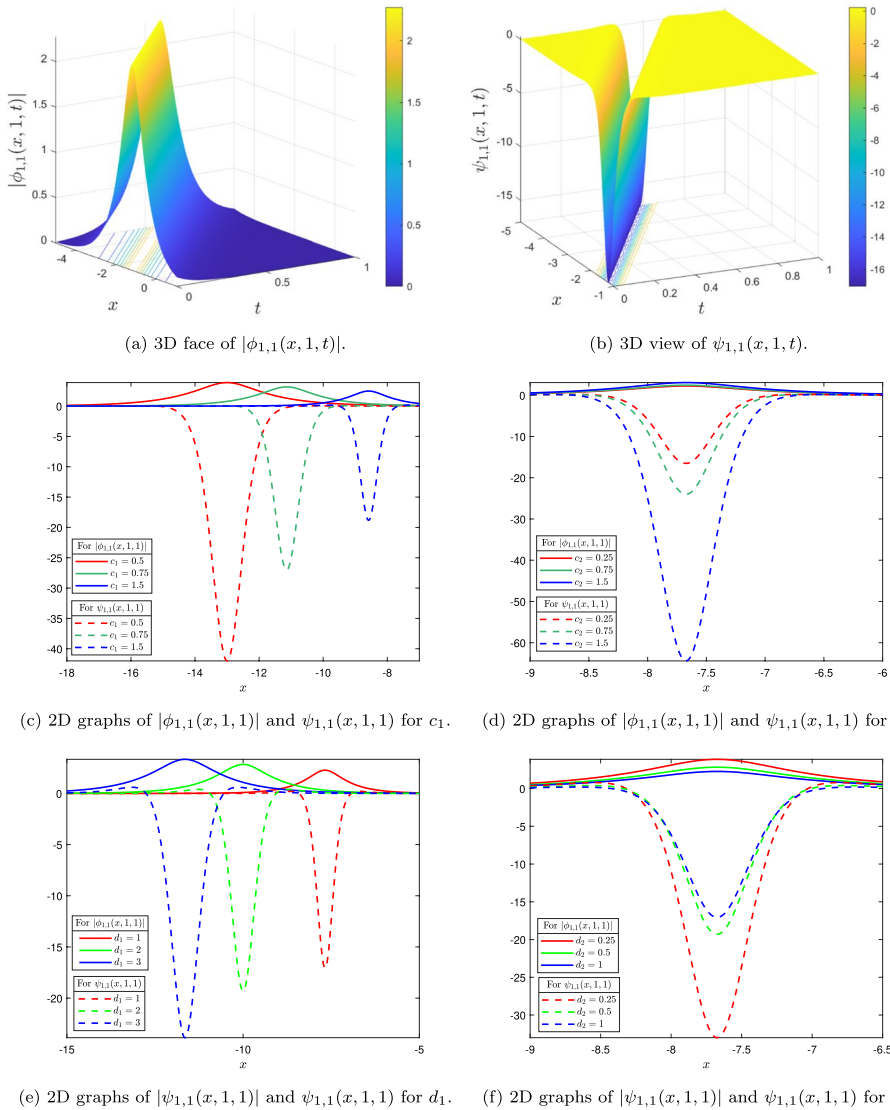
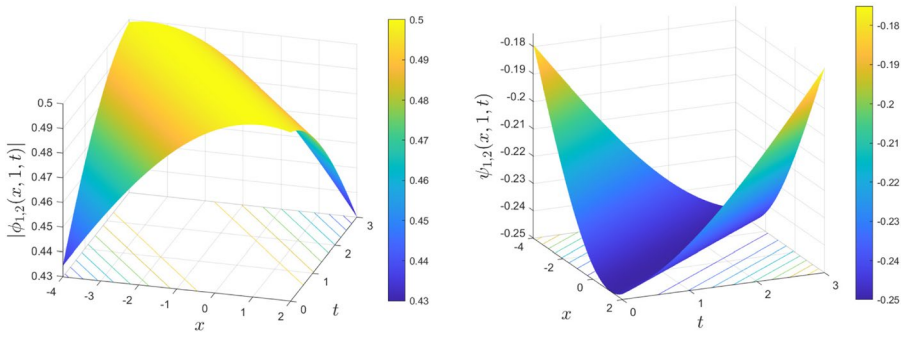


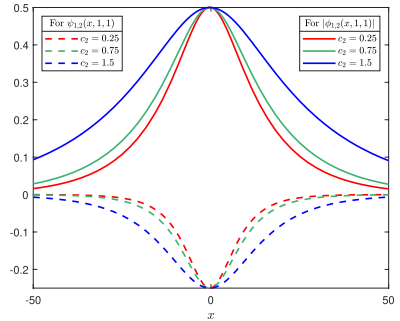
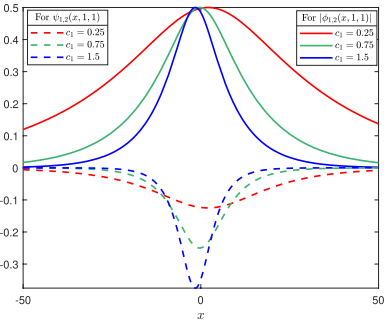
Fig. 1 The graphs of $\phi_{1,1}(x, 1, t)$ and $\psi_{1,1}(x, 1, t)$ in Eqs. (19), (20) under the effects of c_1 , c_2 , d_1 and d_2

We demonstrate the 3D views of $|\phi_{1,2}(x, 1, t)|$ and $\psi_{1,2}(x, 1, t)$ for the parameter values $\tau = 2$, $c_1 = 2$, $d_1 = 1$, $c_2 = 0.3$, $d_2 = 1$, $a = 1$, $b = -0.4$, $\kappa_1 = 2$, $\kappa_2 = 1$, $\alpha = 1$, $\beta = 2$, $\omega = 1$, $\lambda = 16$, $p_2 = 2$, $\Omega = 1$, $\delta = 2$, $\Lambda_1 = 1$ in Fig. 2a and b, respectively. We depict the 2D graphs for $|\phi_{1,2}(x, 1, 1)|$ (continuous lines) and $\psi_{1,2}(x, 1, 1)$ (dashed lines) with $\tau = 2$, $d_1 = 1$, $c_2 = 0.3$, $d_2 = 1$, $a = 1$, $b = -0.4$, $\kappa_1 = 2$, $\kappa_2 = 1$, $\alpha = 1$, $\beta = 2$, $\omega = 1$, $\lambda = 16$, $p_2 = 2$, $\Omega = 1$, $\delta = 2$, $\Lambda_1 = 1$ at $c_1 = 0.25, 0.75, 1.5$ in Fig. 2c. It can be observed from Fig. 1c that depending on the decrease in c_1 , the skirts of the soliton representation for $|\phi_{1,2}(x, 1, 1)|$ open horizontally, and the bright soliton appearance gradually

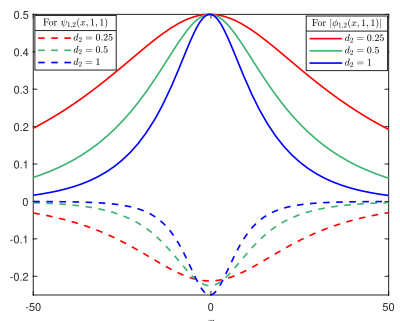
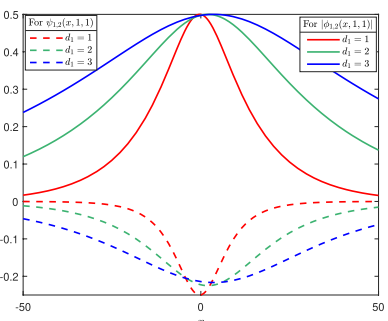
turns into a compacton-like appearance. Moreover, depending on the decrease in c_1 , the dark soliton view for $\psi_{1,2}(x, 1)$ deforms, gradually approaches the horizontal axis (decreases in amplitude), and the apex also shows a position change to the right. For $c_2 = 0.25, 0.75, 1.5$, the 2D plots of $|\phi_{1,2}(x, 1, 1)|$ (continuous lines) and $\psi_{1,2}(x, 1, 1)$ (dashed lines) are illustrated in Fig. 2d at $\tau = 2, c_1 = 2, d_1 = 1, d_2 = 1, a = 1, b = -0.4, \kappa_1 = 2, \kappa_2 = 1, \alpha = 1, \beta = 2, \omega = 1, \lambda = 16, p_2 = 2, \Omega = 1, \delta = 2, \Lambda_1 = 1$. From Fig. 2d we can see inverse effect from Fig. 2c because the skirts of the soliton for $|\phi_{1,2}(x, 1, 1)|$ and $\psi_{1,2}(x, 1, 1)$ open horizontally while c_2 increases. We plot the 2D graphs



(a) 3D portrait of $|\phi_{1,2}(x, 1, t)|$. (b) 3D views of $\psi_{1,2}(x, 1, t)$.



(c) 2D plots of $|\phi_{1,2}(x, 1, 1)|$ and $\psi_{1,2}(x, 1, 1)$ for c_1 . (d) 2D plots of $|\phi_{1,2}(x, 1, 1)|$ and $\psi_{1,2}(x, 1, 1)$ for c_2 .



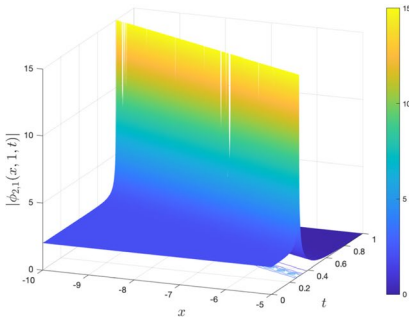
(e) 2D plots of $|\phi_{1,2}(x, 1, 1)|$ and $\psi_{1,2}(x, 1, 1)$ for d_1 . (f) 2D plots of $|\phi_{1,2}(x, 1, 1)|$ and $\psi_{1,2}(x, 1, 1)$ for d_2 .

Fig. 2 The plots of $\phi_{1,2}(x, 1, t)$ and $\psi_{1,2}(x, 1, t)$ in Eqs. (21), (22) under the influences of c_1, c_2, d_1 and d_2

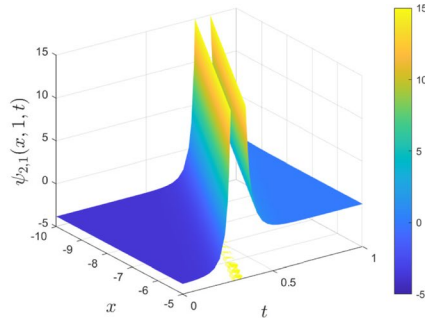
for $|\phi_{1,2}(x, 1, 1)|$ (continuous lines) and $\psi_{1,2}(x, 1, 1)$ (dashed lines) at the values $\tau = 2, c_1 = 2, c_2 = 0.3, d_2 = 1, a = 1, b = -0.4, \kappa_1 = 2, \kappa_2 = 1, \alpha = 1, \beta = 2, \omega = 1, \lambda = 16, p_2 = 2, \Omega = 1, \delta = 2, \Lambda_1 = 1$ for $d_1 = 1, 2, 3$ in Fig. 2e. In Fig. 2e, as d_1 increases, the width of the soliton acquired for $|\phi_{1,2}(x, 1, 1)|$ increases horizontally and the bright soliton view gradually converts to the compacton-like shape. Furthermore, it can be examined from Fig. 2e that the amplitude of the soliton decreases and the apex of the soliton shifts to the right as d_1 increases. Figure 2f shows the 2D views of $|\phi_{1,2}(x, 1, 1)|$ (continuous lines) and $\psi_{1,2}(x, 1, 1)$ (dashed lines) with $\tau = 2, c_1 = 2, d_1 = 1, c_2 = 0.3, a = 1, b = -0.4, \kappa_1 = 2, \kappa_2 = 1, \alpha = 1, \beta = 2, \omega = 1, \lambda = 16, p_2 = 2, \Omega = 1, \delta = 2, \Lambda_1 = 1$ at $d_2 = 0.25, 0.5, 1$. Depending on the decrease in d_2 , the width of the soliton for $|\phi_{1,2}(x, 1, 1)|$ and $\psi_{1,2}(x, 1, 1)$ increases horizontally in Fig. 2f; besides the amplitude of the soliton for $\psi_{1,2}(x, 1, 1)$ (dashed lines) decreases. It can be seen from Fig. 2 that it represents the compacton-like shape.

Figure 3a and b illustrate the 3D plots for $|\phi_{2,1}(x, 1, t)|$ and $\psi_{2,1}(x, 1, t)$ at $\sigma_1 = 2, p_1 = 1, p_2 = 2, \kappa_1 = 0.2, \kappa_2 = 3, a = 0.8, b = 0.2, c_1 = 0.2, c_2 = 0.01, \sigma_1 = 2, p_1 = 1, p_2 = 2, \kappa_1 = 0.2, \kappa_2 = 3, a = 0.8, b = 0.2, c_1 = 0.2, c_2 = 0.01, \alpha = 1, \beta = 0.2, \Omega = -1$, respectively. We depict the 2D plots in Fig. 3c–f so that we examine the effects of the parameters $\kappa_1, \kappa_2, p_1, p_2$ to behavior of the soliton. The 2D views for $|\phi_{2,1}(x, 1, 1)|$ (continuous lines) and $\psi_{2,1}(x, 1, 1)$ (dashed lines) are illustrated in Fig. 3c using the values $\sigma_1 = 2, p_1 = 1, p_2 = 2, \kappa_2 = 3, a = 0.8, b = 0.2, c_1 = 0.2, c_2 = 0.01, \alpha = 1, \beta = 0.2, \Omega = -1$ with $\kappa_1 = 1, 2, 3$. We display the 2D plots of $|\phi_{2,1}(x, 1, 1)|$ (continuous lines) and $\psi_{2,1}(x, 1, 1)$ (dashed lines) in Fig. 3d at $\sigma_1 = 2, p_1 = 1, p_2 = 2, \kappa_1 = 0.2, a = 0.8, b = 0.2, c_1 = 0.2, c_2 = 0.01, \alpha = 1, \beta = 0.2, \Omega = -1$ at $\kappa_2 = 0.25, 0.5, 1$. We demonstrate the 2D views for $|\phi_{2,1}(x, 1, 1)|$ (continuous lines) and $\psi_{2,1}(x, 1, 1)$ (dashed lines) in Fig. 3e with the values $\sigma_1 = 2, p_2 = 2, \kappa_1 = 0.2, \kappa_2 = 3, a = 0.8, b = 0.2, c_1 = 0.2, c_2 = 0.01, \alpha = 1, \beta = 0.2, \Omega = -1$ for $p_1 = 1, 2, 3$. Moreover, the 2D visualizations of $|\phi_{2,1}(x, 1, 1)|$ (continuous lines) and $\psi_{2,1}(x, 1, 1)$ (dashed lines) are plotted in Fig. 3f at $\sigma_1 = 2, p_1 = 1, \kappa_1 = 0.2, \kappa_2 = 3, a = 0.8, b = 0.2, c_1 = 0.2, c_2 = 0.01, \alpha = 1, \beta = 0.2, \Omega = -1$ for $p_2 = 1, 2, 3$. It can be seen from Fig. 3c that depending on the increase in κ_1 , the soliton views for both $|\phi_{2,1}(x, 1, 1)|$ and $\psi_{2,1}(x, 1, 1)$ move to the left. The same effect is observed for κ_2 in Fig. 3d and for p_2 in Fig. 3f. We can examine the inverse effect for p_1 in Fig. 3e because according to the increase in p_1 , the soliton views for both $|\phi_{2,1}(x, 1, 1)|$ and $\psi_{2,1}(x, 1, 1)$ move to the right. We can analyze from Fig. 3 that it shows the singular soliton.

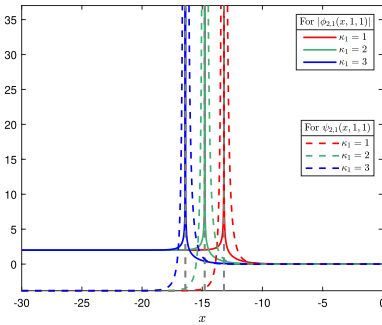
The 3D portraits of $|\phi_{2,2}(x, 1, t)|$ and $\psi_{2,2}(x, 1, t)$ are represented at the parameter values $\sigma_1 = 2, p_1 = 1, p_2 = 2, \kappa_1 = 0.2, \kappa_2 = 3, a = 0.8, \Omega = -1, b = 0.2, c_1 = 0.2, c_2 = 0.01, \alpha = 1, \beta = 0.2$ in Fig. 4a and b, respectively. Figure 4a shows the kink soliton view as Fig. 4b represents the view of a combination of dark and kink soliton. We plot the 2D views of $|\phi_{2,2}(x, 1, 1)|$ (continuous lines) and $\psi_{2,2}(x, 1, 1)$ (dashed lines) at $\sigma_1 = 2, p_1 = 1, p_2 = 2, \kappa_2 = 3, a = 0.8, \Omega = -1, b = 0.2, c_1 = 0.2, c_2 = 0.01, \alpha = 1, \beta = 0.2$ for $\kappa_1 = 0.1, 0.2, 0.3$ in Fig. 4c. We can observe from Fig. 4c that depending on the increasing values of κ_1 in the $|\phi_{2,2}(x, 1, 1)|$ graph, the kink soliton view turns into a smoother form; besides, there is no change in the levels of the lower and upper skirts (flats) of the soliton, that is, in the amplitude of the soliton. For $\psi_{2,2}(x, 1, 1)$, depending on the increase in κ_1 , the kink-dark soliton view does not change in general, but the lower peak (hole) point of the dark soliton shows a position change to the left. However, both the upper side (upper left flatness) and lower side (lower right flatness) of the kink soliton remain at the same level (amplitude) horizontally depending on the decreasing or increasing values of x . The 2D plots for $|\phi_{2,2}(x, 1, 1)|$ (continuous lines) and $\psi_{2,2}(x, 1, 1)$ (dashed lines) are depicted with the values



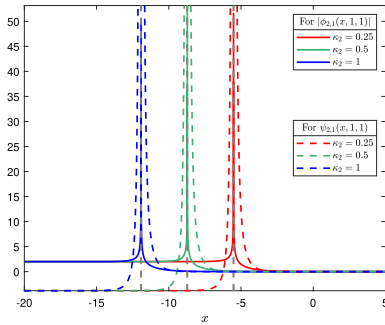
(a) 3D portrait of $|\phi_{2,1}(x, 1, t)|$.



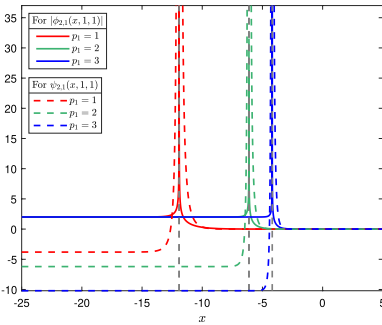
(b) 3D plot of $\psi_{2,1}(x, 1, t)$.



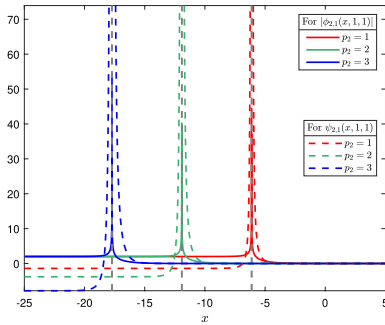
(c) 2D views of $|\phi_{2,1}(x, 1, 1)|$ and $\psi_{2,1}(x, 1, 1)$ for κ_1 .



(d) 2D views of $|\phi_{2,1}(x, 1, 1)|$ and $\psi_{2,1}(x, 1, 1)$ for κ_2 .



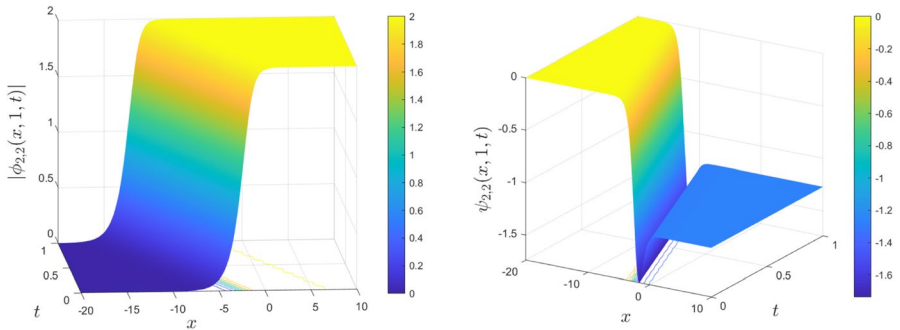
(e) 2D views of $|\phi_{2,1}(x, 1, 1)|$ and $\psi_{2,1}(x, 1, 1)$ for p_1 .



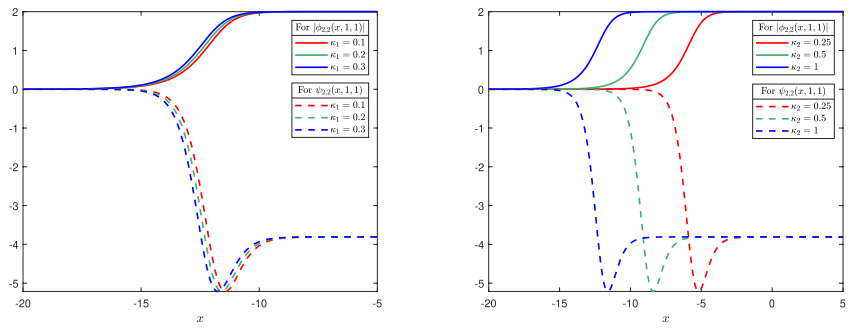
(f) 2D views of $|\phi_{2,1}(x, 1, 1)|$ and $\psi_{2,1}(x, 1, 1)$ for p_2 .

Fig. 3 The plots for $\phi_{2,1}(x, 1, t)$ and $\psi_{2,1}(x, 1, t)$ in Eqs. (36) and (37) under the effects of κ_1 , κ_2 , p_1 and p_2

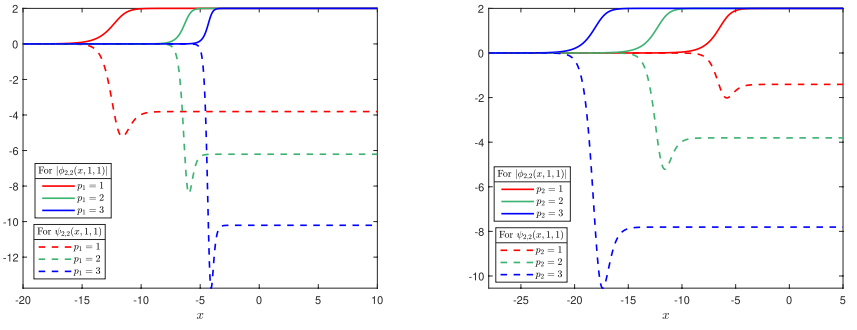
$\sigma_1 = 2, p_1 = 1, p_2 = 2, \kappa_1 = 0.2, a = 0.8, \Omega = -1, b = 0.2, c_1 = 0.2, c_2 = 0.01, \alpha = 1, \beta = 0.2$ for $\kappa_2 = 0.25, 0.5, 1$ in Fig. 4d. It can be understood from Fig. 4d that the kink soliton view for $|\phi_{2,2}(x, 1, 1)|$ is preserved, and the soliton for $|\phi_{2,2}(x, 1, 1)|$ moves to the left depending on the increasing values of κ_2 . The same effect is observed for the soliton view of $\psi_{2,2}(x, 1, 1)$ in Fig. 4d, that is, there is a movement to the left according to an increase in κ_2 . We represent the 2D views of $|\phi_{2,2}(x, 1, 1)|$ (continuous lines) and $\psi_{2,2}(x, 1, 1)$ (dashed lines) in Fig. 4e at the values $\sigma_1 = 2, p_2 = 2, \kappa_1 = 0.2, \kappa_2 = 3, a = 0.8, \Omega = -1, b = 0.2, c_1 = 0.2, c_2 = 0.01, \alpha = 1, \beta = 0.2$ for



(a) 3D portrait of $|\phi_{2,2}(x, 1, t)|$. (b) 3D plot of $\psi_{2,2}(x, 1, t)$.



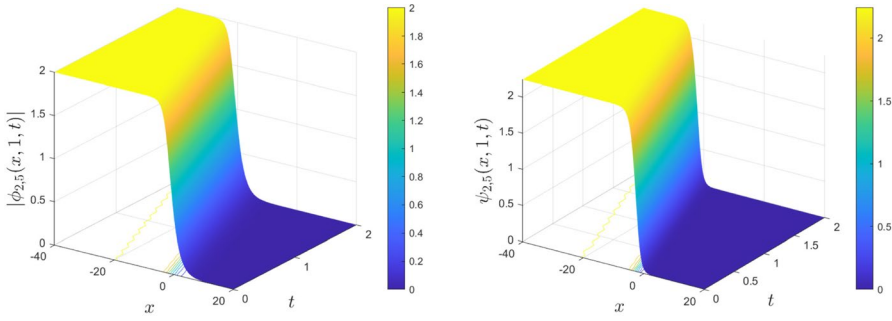
(c) 2D views of $|\phi_{2,2}(x, 1, 1)|$ and $\psi_{2,2}(x, 1, 1)$ for κ_1 . (d) 2D views of $|\phi_{2,2}(x, 1, 1)|$ and $\psi_{2,2}(x, 1, 1)$ for κ_2 .



(e) 2D views of $|\phi_{2,2}(x, 1, 1)|$ and $\psi_{2,2}(x, 1, 1)$ for p_1 . (f) 2D views of $|\phi_{2,2}(x, 1, 1)|$ and $\psi_{2,2}(x, 1, 1)$ for p_2 .

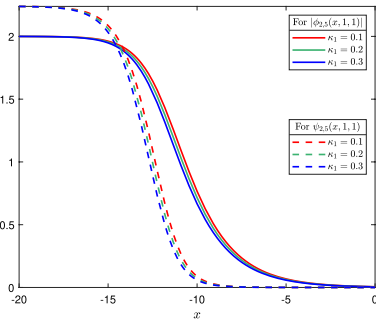
Fig. 4 The plots for $\phi_{2,2}(x, 1, t)$, $\psi_{2,2}(x, 1, t)$ in Eqs. (38) and (39) with the effects of κ_1 , κ_2 , p_1 and p_2

$p_1 = 1, 2, 3$. We can interpret from Fig. 4e that with the increase of p_1 , the soliton for $|\phi_{2,2}(x, 1, 1)|$ (solid lines) changes position to the right, but this change is not proportional to the increase in p_1 (red to green). At the same time, there is no change in the left and right flatness levels of the soliton for $|\phi_{2,2}(x, 1, 1)|$. Moreover, for $\psi_{2,2}(x, 1, 1)$, with the increase of p_1 , the soliton reflects both a rightward movement and a vertical amplitude increase. With a similar interpretation, we can not say that these increments are directly proportional to p_1 . The 2D graphs for $|\phi_{2,2}(x, 1, 1)|$ (continuous lines) and $\psi_{2,2}(x, 1, 1)$ (dashed lines) are displayed in Fig. 4f with

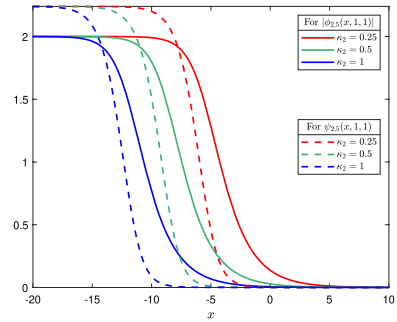


(a) 3D plot of $|\phi_{2,5}(x, 1, t)|$.

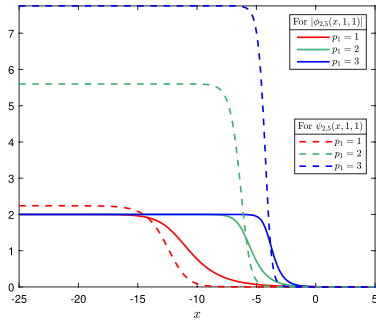
(b) 3D portrait of $\psi_{2,5}(x, 1, t)$.



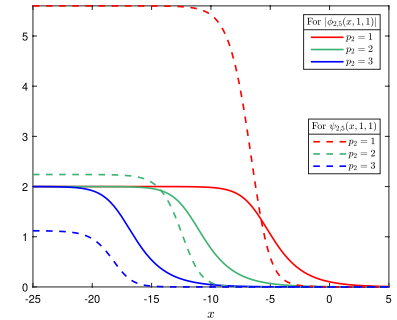
(c) 2D views of $|\phi_{2,5}(x, 1, 1)|$ and $\psi_{2,5}(x, 1, 1)$ for κ_1 .



(d) 2D views of $|\phi_{2,5}(x, 1, 1)|$ and $\psi_{2,5}(x, 1, 1)$ for κ_2 .



(e) 2D views of $|\phi_{2,5}(x, 1, 1)|$ and $\psi_{2,5}(x, 1, 1)$ for p_1 .



(f) 2D views of $|\phi_{2,5}(x, 1, 1)|$ and $\psi_{2,5}(x, 1, 1)$ for p_2 .

Fig. 5 The graphs of $\phi_{2,5}(x, 1, t)$, $\psi_{2,5}(x, 1, t)$ in Eqs. (44), (45) under the effects of κ_1 , κ_2 , p_1 and p_2

$\sigma_1 = 2, p_1 = 1, \kappa_1 = 0.2, \kappa_2 = 3, a = 0.8, \Omega = -1, b = 0.2, c_1 = 0.2, c_2 = 0.01, \alpha = 1, \beta = 0.2$ at $p_2 = 1, 2, 3$. It can be analyzed from Fig. 4f that although the soliton for $|\phi_{2,2}(x, 1, 1)|$ moves to the left, there is no change in the left and right flatness levels of the soliton for $|\phi_{2,2}(x, 1, 1)|$ as in Fig. 4e while p_2 increases. Contrary to Fig. 4e, the soliton for $\psi_{2,2}(x, 1, 1)$ moves to the left with an increase of p_2 . Furthermore, Fig. 4f gives the view of amplitude increment vertically with increment in p_2 .

We represent the 3D portraits of $|\phi_{2,5}(x, 1, t)|$ and $\psi_{2,5}(x, 1, t)$ at $\sigma_1 = 2, Y_1 = 1, p_1 = 1, p_2 = 2, \kappa_1 = 0.1, \kappa_2 = 3, a = 0.8, b = 0.2, \alpha = 1, \beta = 0.4, \Omega = -1$

in Fig. 5a and b, respectively. We can observe that Fig. 5a and b display the kink soliton. In Fig. 5c, the 2D views for $|\phi_{2,5}(x, 1, 1)|$ (continuous lines) and $\psi_{2,5}(x, 1, 1)$ (dashed lines) are depicted using $\sigma_1 = 2, Y_1 = 1, p_1 = 1, p_2 = 2, \kappa_2 = 3, a = 0.8, b = 0.2, \alpha = 1, \beta = 0.4, \Omega = -1$ with $\kappa_1 = 0.1, 0.2, 0.3$. It is seen from Fig. 5c that for both $|\phi_{2,5}(x, 1, 1)|$ graph and $\psi_{2,5}(x, 1, 1)$ graph, the lower and upper flatness levels of the soliton, that is, the amplitude of the soliton, do not change and there is a very small movement to the left with the increase of κ_1 . We illustrate the 2D plots of $|\phi_{2,5}(x, 1, 1)|$ (continuous lines) and $\psi_{2,5}(x, 1, 1)$ (dashed lines) via $\sigma_1 = 2, Y_1 = 1, p_1 = 1, p_2 = 2, \kappa_1 = 0.1, a = 0.8, b = 0.2, \alpha = 1, \beta = 0.4, \Omega = -1$ for $\kappa_2 = 0.25, 0.5, 1$ in Fig. 5d. Similar to the observation in Fig. 5c, it can be interpreted from Fig. 5d that the amplitude of the soliton does not change for both $|\phi_{2,5}(x, 1, 1)|$ graph and $\psi_{2,5}(x, 1, 1)$ graph, while the soliton moves to the left with the increase of κ_2 . Moreover, Fig. 5e demonstrates the 2D views of $|\phi_{2,5}(x, 1, 1)|$ (continuous lines) and $\psi_{2,5}(x, 1, 1)$ (dashed lines) with $\sigma_1 = 2, Y_1 = 1, p_2 = 2, \kappa_1 = 0.1, \kappa_2 = 3, a = 0.8, b = 0.2, \alpha = 1, \beta = 0.4, \Omega = -1$ at $p_1 = 1, 2, 3$. Figure 5e shows that the solitons for both $|\phi_{2,5}(x, 1, 1)|$ and $\psi_{2,5}(x, 1, 1)$ move the the right with the increment of p_1 . Depending on the increase in p_1 , the amplitude of the soliton does not change for $|\phi_{2,5}(x, 1, 1)|$ graph, while the amplitude of the soliton increases for $\psi_{2,5}(x, 1, 1)$ graph according to Fig. 5e. The 2D plots of $|\phi_{2,5}(x, 1, 1)|$ (continuous lines) and $\psi_{2,5}(x, 1, 1)$ (dashed lines) at $\sigma_1 = 2, Y_1 = 1, p_1 = 1, \kappa_1 = 0.1, \kappa_2 = 3, a = 0.8, b = 0.2, \alpha = 1, \beta = 0.4, \Omega = -1$ are depicted for $p_2 = 1, 2, 3$ in Fig. 5f. Unlike Fig. 5e, in 5f, the movement of the soliton is to the left for both $|\phi_{2,5}(x, 1, 1)|$ graph and $\psi_{2,5}(x, 1, 1)$ graph depending on the p_2 increment. Furthermore, with the increment of p_2 , while there is no change in the amplitude of the soliton for $|\phi_{2,5}(x, 1, 1)|$ graph, the amplitude of the soliton decreases for $\psi_{2,5}(x, 1, 1)$ graph in Fig. 5f.

In conclusion for this section, it should be noted that the graphs presented above and the examinations conducted pertain to the parabolic law nonlinearity form of the (2+1)-DSS model, which has been introduced for the first time in this study. In this regard, the results obtained have been presented for the first time in this study. Moreover, before proceeding to the graphic presentations of the conducted studies, it has been verified that all the solution functions obtained satisfy the main equation.

7 Conclusion

In this research article, the (2+1)-dimensional Davey-Stewartson system, which has a distinctive importance among NLPDEs and is the subject of many studies, has been investigated by adapting its parabolic law nonlinearity form. The examination was conducted using two effective methods, nKM and ShGEEM, and bright, dark, singular, and various kink-type soliton solutions were obtained. The 3D and 2D plots of some of the acquired solutions were depicted by using the appropriate parameter values. Moreover, the effect of parameters related to the parabolic law nonlinearity form has been investigated and interpreted with detailed graphical presentations. The acquired results provided us that the generated system is a model that produces different types of solitons and gives analytical solutions. The model that is worked on awaits the researchers' interest to obtain different types of solitons using other methods, to study the fractional forms, to investigate multiple

soliton solutions, to conduct bifurcation analysis, and to research its stochastic forms as open problems in this field.

Author Contributions All parts contained in the research were carried out by the authors through hard work and a review of the various references and contributions in the field of mathematics and Applied physics.

Funding No funding for this article.

Data availability Data sharing is not applicable to this article as no datasets were generated or analyzed during the current study.

Declarations

Conflict of interest This research received no specific grant from any funding agency in the public, commercial or not-for-profit sectors. The authors did not have any competing interests in this research.

Ethical approval The Corresponding Author, declares that this manuscript is original, has not been published before, and is not currently being considered for publication elsewhere. The Corresponding Author confirms that the manuscript has been read and approved by all the named authors and there are no other persons who satisfied the criteria for authorship but are not listed. I further confirm that the order of authors listed in the manuscript has been approved by all of us. We understand that the Corresponding Author is the sole contact for the Editorial process and is responsible for communicating with the other authors about progress, submissions of revisions, and final approval of proofs.

References

- Akbulut, A., Arnous, A.H., Hashemi, M.S., Mirzazadeh, M.: Solitary waves for the generalized nonlinear wave equation in (3+1) dimensions with gas bubbles using the Nucci's reduction, enhanced and modified Kudryashov algorithms. *J. Ocean Eng. Sci.* (2022). <https://doi.org/10.1016/j.joes.2022.07.002>
- Akram, G., Sadaf, M., Arshed, S., Sameen, F.: Bright, dark, kink, singular and periodic soliton solutions of Lakshmanan-Porsezian-Daniel model by generalized projective riccati equations method. *Optik* **241**, 167051 (2021)
- Alabedalhadi, M., Al-Smadi, M., Al-Omari, S., Momani, S.: New optical soliton solutions for coupled resonant Davey-Stewartson system with conformable operator. *Opt. Quantum Electron.* **54**(6), 392 (2022)
- Albayrak, P.: Optical solitons of biswas–milovic model having spatio-temporal dispersion and parabolic law via a couple of kudryashov's schemes. *Optik* 170761 (2023)
- Arnous, A.H.: Optical solitons to the cubic quartic Bragg gratings with anti-cubic nonlinearity using new approach. *Optik* (2022). <https://doi.org/10.1016/j.ijleo.2021.168356>
- Arnous, A.H.: Optical solitons with Biswas-Milovic equation in magneto-optic waveguide having Kudryashov's law of refractive index. *Optik* **247**, 167987 (2021). <https://doi.org/10.1016/j.ijleo.2021.167987>
- Arnous, A.H., Mirzazadeh, M.: Application of the generalized Kudryashov method to the Eckhaus equation. *Nonlinear Anal. Modell. Control.* **21**(5), 577–586 (2016). <https://doi.org/10.15388/NA.2016.5.1>
- Arnous, A.H., Moraru, L.: Optical solitons with the complex Ginzburg-Landau equation with Kudryashov's law of refractive index. *Mathematics* **10**(19), 3456 (2022). <https://doi.org/10.3390/math10193456>
- Arnous, A.H., Mirzazadeh, M., Eslami, M.: Exact solutions of the Drinfel'd-Sokolov-Wilson equation using Bäcklund transformation of Riccati equation and trial function approach. *Pramana J. Phys.* **86**(6), 1153–1160 (2016). <https://doi.org/10.1007/s12043-015-1179-1>
- Arnous, A.H., Mirzazadeh, M., Akinyemi, L., Akbulut, A.: New solitary waves and exact solutions for the fifth-order nonlinear wave equation using two integration techniques. *J. Ocean Eng. Sci.* (2022). <https://doi.org/10.1016/j.joes.2022.02.012>
- Arnous, A.H., Mirzazadeh, M., Akbulut, A., Akinyemi, L.: Optical solutions and conservation laws of the Chen-Lee-Liu equation with Kudryashov's refractive index via two integrable techniques. *Waves Random Complex Media* (2022). <https://doi.org/10.1080/17455030.2022.2045044>

- Arshed, S., Raza, N.: Optical solitons perturbation of Fokas-Lenells equation with full nonlinearity and dual dispersion. *Chin. J. Phys.* **63**, 314–324 (2020). <https://doi.org/10.1016/j.cjph.2019.12.004>
- Arshed, S., Raza, N., Alansari, M.: Soliton solutions of the generalized Davey-Stewartson equation with full nonlinearities via three integrating schemes. *Ain Shams Eng. J.* **12**(3), 3091–3098 (2021)
- Cakicioglu, H., Ozisik, M., Secer, A., Bayram, M.: Stochastic dispersive schrödinger-hirota equation having parabolic law nonlinearity with multiplicative white noise via ito calculus. *Optik* **279**, 170776 (2023)
- Davey, A., Stewartson, K.: Stewartson on three-dimensional packets of surface waves, proceedings of the royal society of London. *A Math. Phys. Sci.* **338**(1613), 101–110 (1974)
- Debnath, L.: *Nonlinear water waves*, (1994)
- Ebadi, G., Krishnan, E., Labidi, M., Zerrad, E., Biswas, A.: Analytical and numerical solutions to the Davey-Stewartson equation with power-law nonlinearity. *Waves Random Complex Med.* **21**(4), 559–590 (2011)
- Ebaid, A., Aly, E.H.: Exact solutions for the transformed reduced ostrovsky equation via the f-expansion method in terms of weierstrass-elliptic and jacobian-elliptic functions. *Wave Motion* **49**(2), 296–308 (2012)
- El-Shiekh, R.M., Gaballah, M.: Solitary wave solutions for the variable-coefficient coupled nonlinear schrödinger equations and davey-stewartson system using modified sine-gordon equation method. *J. Ocean Eng. Sci.* **5**(2), 180–185 (2020)
- El-Shiekh, R.M., Gaballah, M.: Novel solitons and periodic wave solutions for Davey-Stewartson system with variable coefficients. *J. Taibah Univ. Sci.* **14**(1), 783–789 (2020)
- Esen, H., Secer, A., Ozisik, M., Bayram, M.: Analytical soliton solutions of the higher order cubic-quintic nonlinear schrödinger equation and the influence of the model's parameters. *J. Appl. Phys.* **132**(5), 053103 (2022)
- Foroutan, M., Kumar, D., Manafian, J., Hoque, A.: New explicit soliton and other solutions for the conformable fractional Biswas-Milovic equation with Kerr and parabolic nonlinearity through an integration scheme. *Optik* **170**, 190–202 (2018). <https://doi.org/10.1016/j.jpleo.2018.05.129>
- Gaballah, M., El-Shiekh, R. M., Akinyemi, L., Rezazadeh, H.: Novel periodic and optical soliton solutions for davey-stewartson system by generalized jacobi elliptic expansion method. *Int. J. Nonlinear Sci. Numer. Simul.* (2022)
- Guo, J., He, J., Li, M., Mihalache, D.: Exact solutions with elastic interactions for the $(2+1)$ -dimensional extended Kadomtsev-Petviashvili equation. *Nonlinear Dyn.* **101**(4), 2413–2422 (2020)
- Guo, L., Kevrekidis, P.G., He, J.: Asymptotic dynamics of higher-order lumps in the Davey-Stewartson II equation. *J. Phys. A Math. Theor.* **55**(47), 475701 (2022)
- Hereman, W., Zhuang, W.: *Symbolic Computation of Solitons via Hirota's Bilinear Method*. Department of Mathematical and Computer Sciences, Colorado, School of Mines (1994)
- Ismael, H.F., Atas, S.S., Bulut, H., Osman, M.: Analytical solutions to the m-derivative resonant Davey-Stewartson equations. *Modern Phys. Lett. B* **35**(30), 2150455 (2021)
- Ismael, H.F., Sulaiman, T.A., Yusuf, A., Bulut, H.: Resonant Davey-Stewartson system: dark, bright mixed dark-bright optical and other soliton solutions. *Opt. Quantum Electron.* **55**(1), 48 (2023)
- Jafari, H., Sooraki, A., Talebi, Y., Biswas, A.: The first integral method and traveling wave solutions to Davey-Stewartson equation. *Nonlinear Anal. Modell. Control* **17**(2), 182–193 (2012)
- Javid, A., Raza, N.: Chiral solitons of the $(1+2)$ -dimensional nonlinear Schrodinger's equation. *Modern Phys. Lett. B* (2019). <https://doi.org/10.1142/S0217984919504013>
- Kudryashov, N.A.: Method for finding highly dispersive optical solitons of nonlinear differential equations. *Optik* **206**, 163550 (2020)
- Kumar, D., Manafian, J., Hawlader, F., Ranjbaran, A.: New closed form soliton and other solutions of the Kundu-Eckhaus equation via the extended Sinh-Gordon equation expansion method. *Optik* **160**, 159–167 (2018). <https://doi.org/10.1016/j.jpleo.2018.01.137>
- Kumar, D., Seadawy, A.R., Chowdhury, R.: On new complex soliton structures of the nonlinear partial differential equation describing the pulse narrowing nonlinear transmission lines. *Opt. Quantum Electron.* **50**(2), 1–14 (2018). <https://doi.org/10.1007/s11082-018-1383-6>
- Kumar, D., Joardar, A.K., Hoque, A., Paul, G.C.: Investigation of dynamics of nematons in liquid crystals by extended sinh-Gordon equation expansion method. *Opt. Quantum Electron.* **51**(7), 1–36 (2019). <https://doi.org/10.1007/s11082-019-1917-6>
- Liang, Z., Tang, X.: Painlevé analysis and exact solutions of the resonant Davey-Stewartson system. *Phys. Lett. A* **374**(2), 110–115 (2009)
- Li, B., Ye, W.-C., Chen, Y.: Symmetry, full symmetry groups, and some exact solutions to a generalized Davey-Stewartson system. *J. Math. Phys.* **49**(10), 103503 (2008)

- Mathanaranjan, T., Kumar, D., Rezazadeh, H., Akinyemi, L.: Optical solitons in metamaterials with third and fourth order dispersions. *Opt. Quantum Electron.* **54**(5), 1–15 (2022). <https://doi.org/10.1007/s11082-022-03656-1>
- Mirzazadeh, M., Eslami, M., Arnous, A.H.: Dark optical solitons of Biswas-Milovic equation with dual-power law nonlinearity. *Eur. Phys. J. Plus* **130**(1), 1–7 (2015). <https://doi.org/10.1140/epjp/i2015-15004-x>
- Onder, I., Secer, A., Ozisik, M., Bayram, M.: Obtaining optical soliton solutions of the cubic-quartic Fokas-Lenells equation via three different analytical methods. *Opt. Quantum Electron.* **54**(12), 786 (2022)
- Ozdemir, N.: Optical solitons for Radhakrishnan-Kundu-Lakshmanan equation in the presence of perturbation term and having kerr law. *Optik* **271**, 170127 (2022)
- Ozisik, M.: Novel $(2+1)$ and $(3+1)$ forms of the Biswas-Milovic equation and optical soliton solutions via two efficient techniques. *Optik* **269**, 169798 (2022)
- Ozisik, M., Bayram, M., Secer, A., Cinar, M.: Solitons in dual-core optical fibers with chromatic dispersion. *Opt. Quantum Electron.* **55**(2), 162 (2023)
- Ozisik, M., Secer, A., Bayram, M., Aydin, H.: An encyclopedia of kudryashov's integrability approaches applicable to optoelectronic devices. *Optik* **265**, 169499 (2022)
- Ozisik, M., Onder, I., Esen, H., Cinar, M., Ozdemir, N., Secer, A., Bayram, M.: On the investigation of optical soliton solutions of cubic-quartic Fokas-Lenells and schrödinger-Hirota equations. *Optik* **272**, 170389 (2023)
- Peregrine, D.H.: Water waves, nonlinear schrödinger equations and their solutions. *ANZIAM J.* **25**(1), 16–43 (1983)
- Raza, N., Javid, A.: Optical dark and dark-singular soliton solutions of $(1+2)$ -dimensional chiral nonlinear Schrodinger's equation. *Waves Random Complex Med.* **29**(3), 496–508 (2019). <https://doi.org/10.1080/17455030.2018.1451009>
- Raza, N., Afzal, U., Butt, A.R., Rezazadeh, H.: Optical solitons in nematic liquid crystals with Kerr and parabolic law nonlinearities. *Opt. Quantum Electron.* **51**(4), 1–16 (2019). <https://doi.org/10.1007/s11082-019-1813-0>
- Raza, N., Javid, A., Butt, A.R., Baskonus, H.M.: Optical solitons and stability regions of the higher order nonlinear Schrödinger's equation in an inhomogeneous fiber. *Int. J. Nonlinear Sci. Numer. Simul.* **24**(2), 567–579 (2023). <https://doi.org/10.1515/ijnsns-2021-0165>
- Satsuma, J.: Hirota bilinear method for nonlinear evolution equations. In: *Direct and Inverse Methods in Nonlinear Evolution Equations: Lectures Given at the CIME Summer School Held in Cetraro, Italy, September 5-12, 1999*, Springer, pp. 171–222 (2003)
- Seadawy, A.R., Kumar, D., Chakrabarty, A.K.: Dispersive optical soliton solutions for the hyperbolic and cubic-quintic nonlinear Schrödinger equations via the extended sinh-Gordon equation expansion method. *Eur. Phys. J. Plus* **133**(5), 1–11 (2018). <https://doi.org/10.1140/epjp/i2018-12027-9>
- Selima, E.S., Seadawy, A.R., Yao, X.: The nonlinear dispersive davey-stewartson system for surface waves propagation in shallow water and its stability. *Eur. Phys. J. Plus* **131**, 1–16 (2016)
- Shahoot, A., Alurffi, K., Hassan, I., Almsri, A.: Solitons and other exact solutions for two nonlinear pdes in mathematical physics using the generalized projective riccati equations method. *Adv. Math. Phys.* (2018)
- Sun, Y., Tian, B., Yuan, Y.-Q., Du, Z.: Semi-rational solutions for a $(2+1)$ -dimensional davey-stewartson system on the surface water waves of finite depth. *Nonlinear Dyn.* **94**, 3029–3040 (2018)
- Tang, X., Chow, K., Rogers, C.: Propagating wave patterns for the 'Resonant'davey-Stewartson system. *Chaos Solitons Fractals* **42**(5), 2707–2712 (2009)
- Whitham, G. B.: *Linear and nonlinear waves*. Wiley (2011)
- Yan, Z.: Jacobi elliptic function solutions of nonlinear wave equations via the new Sinh-Gordon equation expansion method. *J. Phys. A Math. General* **36**(7), 1961 (2003)
- Yan, Z.: A sinh-gordon equation expansion method to construct doubly periodic solutions for nonlinear differential equations. *Chaos Solitons Fractals* **16**(2), 291–297 (2003)
- Yıldırım, Y.: Optical solitons with biswas-arsheed equation by f-expansion method. *Optik* **227**, 165788 (2021)
- Zedan, H.A., Monaquel, S.J.: The sine-cosine method for the davey-stewartson equations. *Appl. Math. E-Notes* **10**, 103–111 (2010)
- Zhao, Y.-M.: F-expansion method and its application for finding new exact solutions to the kudryashov-sinelshchikov equation. *J. Appl. Math.* (2013)

Springer Nature or its licensor (e.g. a society or other partner) holds exclusive rights to this article under a publishing agreement with the author(s) or other rightsholder(s); author self-archiving of the accepted manuscript version of this article is solely governed by the terms of such publishing agreement and applicable law.